Investigation of microstructure changes in Al2O3-YSZ coatings and YSZ coatings and their effect on thermal cycle life

Meiqi Dai
State Key Laboratory of High Performance Ceramics and Superfine Microstructure Shanghai Institute of Ceramics Chinese Academy of Sciences

Xuemei Song
State Key Laboratory of High Performance Ceramics and Superfine Microstructure Shanghai Institute of Ceramics Chinese Academy of Sciences

Chucheng Lin
State Key Laboratory of High Performance Ceramics and Superfine Microstructure Shanghai Institute of Ceramics Chinese Academy of Sciences

Ziwei Liu
State Key Laboratory of High Performance Ceramics and Superfine Microstructure Shanghai Institute of Ceramics Chinese Academy of Sciences

Wei Zheng
State Key Laboratory of High Performance Ceramics and Superfine Microstructure Shanghai Institute of Ceramics Chinese Academy of Sciences

Yi Zeng (zengyi@mail.sic.ac.cn)
Shanghai Institute of Ceramics, Chinese Academy of Science

Research Article

Keywords: Thermal barrier coatings, Thermal cycling, Microstructure change, Microscopic strain, Failure mechanism

Posted Date: May 11th, 2021

DOI: https://doi.org/10.21203/rs.3.rs-506350/v1

Version of Record: A version of this preprint was published at Journal of Advanced Ceramics on January 11th, 2022. See the published version at https://doi.org/10.1007/s40145-021-0538-2.

Abstract

Yttria-stabilized zirconia (YSZ) coatings and Al_2O_3-YSZ coatings were prepared by atmospheric plasma spraying (APS). Their microstructural changes during thermal cycling were investigated via scanning electron microscopy (SEM) equipped with electron backscatter diffraction (EBSD) and X-ray diffraction (XRD). It was found that the microstructure and microstructure changes of the two coatings were different, including crystallinity, grain orientation, phase, and phase transition. These differences are closely related to the thermal cycle life of the coating. There is a relationship between crystallinity and crack size. Changes in grain orientation are related to microscopic strain and cracks. Phase transition is the direct cause of coating failure. In this study, the relationship between the changes in the coating microstructure and the thermal cycle life is discussed in detail. The failure mechanism of the coating was comprehensively analyzed from a microscopic perspective.

1. Introduction

Thermal barrier coatings (TBCs) are widely used in hot-end parts such as gas turbine blades in the aerospace field to provide protection for superalloys so that they can work at higher intake temperatures. The ultimate goal of TBCs is to improve the thrust of the aero-engine and the thermal efficiency of the fuel [1–4]. However, turbine inlet temperature requirements are continuously increasing with continuous development in the aerospace field. Traditional YSZ coatings cannot meet the requirements of high-performance aero-engines owing to their high thermal conductivity and poor thermal stability [5–7]. Therefore, in recent years, numerous studies have focused on developing new TBC systems with lower thermal conductivity, including doping other metal oxides such as Sc_2O_3, Al_2O_3, CeO_2, SnO_2, La_2O_3, Gd_2O_3, Yb_2O_3 into YSZ coatings [8]. Among these metal oxides doped materials, Al_2O_3-YSZ coating is expected to become a candidate material for TBCs owing to its excellent performance. Al_2O_3-YSZ coatings prepared by Tarasi et al. and Song et al. [9, 10] had low thermal conductivities of 0.99 W/m·K and 0.91 W/m·K at room temperature, respectively, which were lower than that of YSZ coating. Yu et al. [11] prepared nanostructured 13 wt% Al_2O_3-8 wt% Y_2O_3-ZrO_2(13AlYSZ) coatings by atmospheric plasma spraying. The addition of nano-Al_2O_3 effectively restrained the grain growth of the zirconia phase and improved the thermal stability of the coating at high temperatures. Yin et al. [12] studied the corrosion resistance and mechanical properties of Al_2O_3-modified YSZ coatings. It was found that Al_2O_3 doping could prevent CMAS corrosion due to the formation of anorthite.

It should be noted that regardless of the performance of the coating, the thermal cycle life determines whether the coating can be applied in practice. According to related references and experimental results, Al_2O_3-YSZ coating can have thermal cycle life which is almost as long as its YSZ counterpart by the design of double-layer coating [13]. So it is crucial to investigate the factors to influence the thermal cycle life. However, current research on the thermal cycle life of TBCs is mainly focused on macroscopic stress, concentrating on the thermal expansion coefficient or residual stress [14–16]. Xu et al.[17] established the relationship between the thermal expansion coefficient and the Al_2O_3 doping amount. They found that

the thermal expansion coefficient shows a downward trend with an increasing amount of Al_2O_3 doping. Song et al. [18]found that the change in thermal expansion coefficient caused by Al_2O_3 doping could be attributed to the change in lattice constant, which leads to a change in the bonding strength of Al_2O_3-doped t-YSZ. Wang et al. [19]attributed delamination failure of the coating to the large stress induced by the appearance of the thermally grown oxide. However, few studies have explored the effect of the microstructure and its changes on the thermal cycle life of the coating from a microscopic point of view. The change in grains and microscopic stress produced during thermal cycling are often ignored. According to finite element simulation, the magnitude of the numerical change in the microscopic stress is at the MPa level, and it could even reach the GPa level in some cases [20–22]. Therefore, the influence of microscopic stress on the thermal cycle life of the coating cannot be ignored.

In this study, YSZ and Al_2O_3-YSZ coatings were prepared by atmospheric plasma spraying (APS) technology. The same position was analyzed by scanning electron microscopy (SEM) equipped with electron backscatter diffraction (EBSD) to determine the microstructural changes occurring during thermal cycling. By comparing the microstructure of the two coatings and the changes in microstructure during thermal cycling, the failure mechanism of the coating was analyzed by microscopic strain and phase transition.

2. Experimental Procedures

2.1 Materials and coating preparation

In this experiment, the TBC system includes a metal substrate, a metal bonding layer, and a ceramic layer. A Ni-based superalloy was selected as the metal substrate, and cuboid samples with dimensions of 20 mm × 10 mm × 2 mm were prepared. A bonding layer with a thickness of 100 μm was prepared by vacuum plasma spraying (VPS – Sulzer Metco AG, Switzerland), which was used to connect the ceramic layer and the substrate. The chemical composition of the bonding layer powders is listed in Table 1. Commercial YSZ powder (7.5 wt% Y_2O_3) and Al_2O_3-YSZ powder (10 wt% Al_2O_3, 7.5 wt% Y_2O_3) were used to prepare the ceramic layer with a thickness of 200 μm by APS (Sulzer Metco AG, Switzerland). Table 2 lists the spraying parameters used.

Table 1
Chemical composition of NiCrCoAlY powder in bond coat (wt%)

Element	Co	Ni	Cr	Al	Y
Content	Bal.	29.0–35.0	29.0–35.0	5.0–11.0	0.1–0.8

Table 2
Parameters of plasma spraying

Parameter	Bond coat	Ceramic topcoat
Spraying process	VPS	APS
Current/A	720	600
Ar/(L min^{-1})	50	30
H_2/(L min^{-1})	9	10
Spray distance/mm	275	120

2.2 Thermal cycling test

The purpose of the thermal cycling experiments was to understand the changes in coating microstructure that occur with temperature changes. First, the two samples were placed in a tube furnace at 950°C for 15 min, and then they were removed and placed in air for 25 min to cool the samples to near room temperature [23]. The two samples were characterized after different numbers of thermal cycles (0, 5, 10, 15, 20, 25, 30, and 40).

2.3 Ex-situ characterization and calculation of misorientation

For the thermal cycling experiments of the YSZ and Al_2O_3-YSZ coatings, one area was selected in the two coatings' cross-sections for ex-situ characterization. The microstructure of the coating was observed using a field emission scanning electron microscope (Magellan 400, FEI, USA) equipped with an EBSD probe (INCA SERIES, Oxford Instrument, UK). While obtaining the morphology information, the orientation information of each grain was also included, which was expressed in the form of three Euler angles. In this experiment, the orientation change of some randomly selected grains during thermal cycling was calculated, and the detailed process is as follows. First, two groups of Euler angles before and after thermal cycling of the same grain were transformed into an orientation matrix. The transition formulas of the Euler angle (φ_1, Φ, φ_2) and orientation matrix are as follows:

$\cos\varphi_1\cos\varphi_2-\sin\varphi_1\sin\varphi_2\cos\Phi$	$\sin\varphi_1\cos\varphi_2+\cos\varphi_1\sin\varphi_2\cos\Phi$	$\sin\varphi_2\sin\Phi$
$-\cos\varphi_1\sin\varphi_2-\sin\varphi_1\cos\varphi_2\cos\Phi$	$-\sin\varphi_1\sin\varphi_2+\cos\varphi_1\cos\varphi_2\cos\Phi$	$\cos\varphi_2\sin\Phi$
$\sin\varphi_1\sin\Phi$	$-\cos\varphi_1\sin\Phi$	$\cos\Phi$

The relationship between $\mathbf{M_1}$ and $\mathbf{M_2}$ can be defined as follows: $\mathbf{M_2} = \mathbf{M_{1\to2}}\cdot\mathbf{M_1}$ or $\mathbf{M_{1\to2}}=\mathbf{M_2}^{-1}\cdot\mathbf{M_1}$. $\mathbf{M_{1\to2}}$ is a disorientation matrix. $\mathbf{M_2}^{-1}$ is the inverse matrix of $\mathbf{M_2}$. In this work, matrix $\mathbf{M_{1\to2}}$ was converted to the rotation axis and rotation angle. The rotation angle was used as the criterion to evaluate the degree of grain orientation change. The formula for calculating the rotation angle is as follows:

$$\text{theta} = \arccos(0.5\times(\mathbf{M_{1\to2}}\,\mathbf{11} + \mathbf{M_{1\to2}}\,\mathbf{22} + \mathbf{M_{1\to2}}\,\mathbf{33} - 1))$$

The phase composition and micro-strain of the coating at different thermal cycles were characterized using a two-dimensional micro-focal spot X-ray diffractometer (D8 ADVANCE, Bruker, Germany).

3. Experimental Results

3.1 Microstructure of the as-sprayed YSZ and Al_2O_3-YSZ coatings before thermal cycling

The X-ray diffraction (XRD) patterns of the YSZ and Al_2O_3-YSZ coatings before thermal cycling are shown in Fig. 1. At high magnification of the XRD patterns, it can be seen that there is a unique peak from the tetragonal phase in the YSZ coating at approximately 43° when the two patterns are compared. This peak appears only when the content of the tetragonal phase is high. The tetragonal phase can also be characterized by the splitting of multiple peaks from those of the cubic phase. Therefore, the YSZ coating is mainly composed of a tetragonal phase and a small amount of cubic phase. However, doping with 10% Al_2O_3 affects the crystal phase of zirconia, which is mainly composed of a cubic phase and a small amount of tetragonal phase at low temperature. It was found that there is no α-Al_2O_3 phase, which can be explained by a solid solution of some Al atoms in ZrO_2 during plasma spraying [11]and aggregation of some Al atoms at grain boundaries to form amorphous phase [17].

Figure 2 shows the backscattered electron image of the microstructure of the sprayed YSZ and Al_2O_3-YSZ coatings. It can be seen that there are significant differences in microstructure between the two coatings. Through calculations using image processing software, the average crack size in the Al_2O_3-YSZ coating was determined to be 5.6 μm^2 and that of the YSZ coating 2.5 μm^2. The principal stress at the crack tip increases with an increase in crack size [24]. According to Griffith's theory of microcracks, the strength of materials does not depend on the number of cracks but on the size of cracks. Once a crack exceeds the critical size, the crack will propagate and connect rapidly, which has an adverse effect on the thermal

cycle life of the coating. An analysis of the experimental data shows that there is a close relationship between crack size and crystallinity.

By calculating the crystallinity of the two coatings, it was found that the crystallinity of the YSZ coating is very high, close to 100 %, while the crystallinity of the Al_2O_3-YSZ coating is 78.56%. As shown in Fig. 3, the crystallinity in different regions of the coating is different. The EBSD scanning and backscattered electron images of the Al_2O_3-YSZ coating in the same area were compared. It was found that the size of the larger cracks in the EBSD scan is significantly larger than that in the backscattered electron image. This phenomenon indicates that an amorphous phase exists near the crack. Along the direction of the arrow, the grain size gradually decreases. In short, there is a gradual transition to the amorphous phase near the crack. When the crystallinity is poor, stress concentration and tensile stress will occur [25]. Therefore, poor crystallinity is the main reason for the formation of large cracks.

3.2 Effect of grain orientation variation and grain morphology on thermal cycle life

3.2.1 Grain orientation variation

Figure 4 shows backscattered electron images of the YSZ and Al_2O_3-YSZ coatings before and after five thermal cycles. After five thermal cycles, there is no obvious change in the microstructure of the YSZ coating, but there is obvious crack propagation and connection in the Al_2O_3-YSZ coating. This experiment was conducted from a microscopic perspective. The experimental data show that the difference between the two coatings is not only related to a larger crack size, but also closely related to the micro-stress.

Approximately ten grains were randomly selected from the EBSD scans of the YSZ and Al_2O_3-YSZ coatings. As shown in Fig. 5 (a) and (b), the disorientation of these ten grains compared with the previous thermal cycle was calculated based on the Euler angle data provided by the software. It was found that the change in degree of orientation of each grain in the two kinds of coatings showed the same trend during the thermal cycles. This is because the grains need to coordinate with the surrounding grains in the process of micro-strain and maintain stress/strain coordination between the various parts [26]. During five thermal cycles, the average change in grain orientation of the YSZ coating was 1.49°, and that of the Al_2O_3-YSZ coating was 5.42°. Comparing the grain orientation change trend diagram of Fig. 5(b) with the micro-strain diagram of Fig. 6(c), it can be seen that the degree of grain orientation change is positively correlated with the micro-strain. This indicates that the degree of change in grain orientation is representative. Therefore, during five thermal cycles, the Al_2O_3-YSZ coating has a large micro-strain, and the resulting micro-stress is of the order of magnitude of MPa. A larger micro-strain promotes crack propagation and connection, which is unfavorable to the thermal cycle life of the coating.

3.2.2 Grain morphology

On closer analysis of the propagation cracks, it was found that different grain shapes have different effects on crack propagation. In this experiment, two regions (site 1 and site 2) near the crack were

selected and characterized by EBSD, as shown in Fig. 6. Compared to Fig. 4(e), it can be seen that a new crack appears in the equiaxed grain region. From the different grain orientations on both sides of the crack, it can be observed that the propagation mode of the crack in the equiaxed grain region is intergranular. The crack in the columnar region propagates further, based on the original crack. The same grain orientation on both sides of the crack indicates that the crack propagates in transgranular mode in the columnar grain region. It is well known that transgranular crack propagation needs to consume more fracture energy, so transgranular cracks are less likely to occur. From Figs. 4(f) and 6(c), it can be seen that the transgranular crack separates into two cracks during propagation, which eases the stress concentration at the crack tip [27]. In contrast, intergranular cracks are more likely to occur when the energy at the grain boundary is high and the atoms are in an unstable state. This is consistent with the fact that transgranular cracks in the columnar grains only occur as the propagation of an original crack, while new cracks appear at equiaxed grains. In general, the existence of columnar grains blocks crack propagation to a certain extent.

The reason for different crack propagation forms in different regions is that the microscopic stress concentration regions of equiaxed and columnar grains are different after the occurrence of micro-strain. As shown in Fig. 6(g), the microscopic stress concentration at the equiaxed grain exists at the grain boundary, which affects the bonding of the grain boundary at the equiaxed grain. From a comparison of Fig. 7 (a) and (b), it is obvious that the equiaxed grains exhibit high and low fluctuations, and there are voids at the grain boundary, especially at the junction of multiple grains. This is consistent with the fact that the crack propagates along equiaxed grains. However, as shown in Fig. 6(d), there is a high probability of stress concentration within the grain after micro-strain of the columnar grains occurs. There is also high energy inside the columnar grains, so the strength difference between the grain boundaries and grains decreases, and the cracks propagate through the columnar grains. In addition, the cracks in the columnar grains are horizontal cracks, which increase the propagation path of vertical cracks and block the penetration of the cracks to a certain extent.

So, a larger micro-strain generates a larger micro-stress, which makes it easier for the cracks to expand and connect, and is not conducive to the thermal cycle life of the coating. Compared with equiaxed grains, columnar grains play a role in blocking the penetration of cracks on the coating to a certain extent.

3.3 Effect of phase and phase transition on thermal cycle life

Figure 8 shows the macroscopic morphology of the coating during thermal cycling. Although crack connection and propagation occurred during five thermal cycles, the coating did not peel off. The most serious spalling occurred after 5–10 thermal cycles. As shown in Fig. 9, the unique peak appears at approximately 43° and the peak splitting occurs at approximately 73° after 10 thermal cycles. Therefore, it can be seen from the XRD analysis that the coating is transformed from the cubic phase to the tetragonal phase during these 5–10 thermal cycles. The crystal transition from c-ZrO_2 to t-ZrO_2 is a displacement transition without interatomic diffusion. There is a 2% volume shrinkage in the transition

from the cubic to the tetragonal zirconia phase [28]. Phase transition coupled with the existing cracks throughout the coating lead to the most serious spalling of the coating during this period.

In addition, a change in grain orientation during thermal cycling of the Al_2O_3–YSZ coating is observed in Fig. 5(b). It can be seen that 10 thermal cycles mark a significant change. From the 10th thermal cycle onward, the degree of change in the grain orientation of the Al_2O_3-YSZ coating is reduced to approximately 1.5°, which is similar to that of the YSZ coating. Correspondingly, the micro-strain of the Al_2O_3–YSZ coating after 10 thermal cycles is also small. The important reason for the difference in the micro-strain before and after thermal cycling is that the toughness and strength of the zirconia tetragonal phase are better than those of the cubic phase [29]. Therefore, it is more difficult for micro-strain of the grains to occur, and the micro-stress generated is relatively small. It can also be seen in Fig. 8 that the exfoliation rate of the coating slows down after 10 thermal cycles. This confirms that micro-stress has an important influence on the thermal cycle life of the coating.

It can be seen that small changes in grain orientation of YSZ coating are due not only to a difference in thermal expansion coefficient, which leads to a difference in thermal stress, but also to the main phase of YSZ coating being the tetragonal phase from beginning to end, so that there is no phase transition process.

4. Conclusion

In this study, two types of TBCs, YSZ and Al_2O_3-YSZ coatings, were prepared. The changes in the microstructure before and during thermal treatment were compared. The entire failure process and factors influencing the thermal cycle life of the coating during thermal cycles were comprehensively analyzed. The results are as follows:

(1) The large crack size is attributed to the appearance of an amorphous phase, which is more likely to expand during thermal cycling. Therefore, low crystallinity is not conducive to the thermal cycle life of the coating.

(2) The micro-stress caused by the large micro-strain of the coating during thermal cycling promotes crack propagation and connection. And the grain morphology affects the microscopic stress concentration area, thus affecting crack propagation.

(3) A transition from the cubic phase to the tetragonal phase, combined with connected cracks, is the direct cause of spalling failure of the coating. However, tetragonal zirconia has less micro-strain in thermal cycling, which can slow down spalling of the coating.

Declarations

Acknowledgments

This work is supported by National Key R&D Program of China (2018YFB0704400), the Shanghai Sailing Program (18YF1427000), the Research Project of Shanghai Science and Technology Committee (19142200600), Shanghai Technical Platform for Testing on Inorganic Materials (19DZ2290700) and the National Nature Science Foundation of China (81672131 and 81871754).

References

[1] Padture NP, Gell M, Jordan EH. Thermal barrier coatings for gas-turbine engine applications. *Science* 2002, **96**: 280-284.

[2] Fleck NA, Cocks ACF, Lampenscherf S. Thermal shock resistance of air plasma sprayed thermal barrier coatings. *J Eur Ceram Soc* 2014, **34**: 2687-2694.

[3] Zhou X, Chen T, Yuan JY, *et al*. Failure of plasma sprayed nano-zirconia-based thermal barrier coatings exposed to molten CaO–MgO–Al_2O_3–SiO_2 deposits. *J Am Ceram Soc* 2019, **102**: 6357-6371.

[4] Cai J, Lv P, Guan QF, *et al*. Thermal cycling behavior of thermal barrier coatings with MCrAlY bond coat irradiated by high-current pulsed electron beam. *ACS Appl Mater Interfaces* 2016, **8**: 32541-32556.

[5] Stöver D, Pracht G, Lehmann H, *et al*. New Material Concepts for the Next Generation of Plasma-Sprayed Thermal Barrier Coatings. *J Therm Spray Technol* 2004, **13**: 76-83.

[6] Cao XQ, Zhang YF, Zhang JF, *et al*. Failure of the plasma-sprayed coating of lanthanum hexaluminate. *J Eur Ceram Soc* 2008, **28**: 1979-1986.

[7] Clarke DR, Levi CG. Materials design for the next generation thermal barrier coatings. *Annu Rev Mater Res* 2003, **33**: 383-417.

[8] Wei XD, Hou GL, Zhao D, *et al*. Recent Research Progress on Oxide Doped YSZ Thermal Barrier Coatings. *SurfTechnol*. 2020, **49**: 92-103

[9] Tarasi F, Medraj M, Dolatabadi A, *et al*. High-temperature performance of alumina-zirconia composite coatings containing amorphous phases. *Adv Funct Mater* 2011, **21**: 4143-4151.

[10] Song XM, Liu ZW, Kong MG, *et al*. Effect of Microstructure on the Thermal Conductivity of Plasma-Sprayed Al_2O_3-YSZ Coatings. *J Therm Spray Technol* 2016, **25**: 770-777.

[11] Yu Q, Zhou C, Zhang HY, *et al*. Thermal stability of nanostructured 13 wt% Al_2O_3-8 wt% Y_2O_3-ZrO_2 thermal barrier coatings. *J Eur Ceram Soc* 2010, **30**: 889-897.

[12] Yin BB, Zhang F, Zhu W, *et al*. Effect of Al_2O_3 modification on the properties of YSZ: Corrosion resistant, wetting and thermal-mechanical properties. *Surf Coatings Technol* 2019, **357**: 161-171.

[13] Song XM, Zhang JM, Liu ZW, *et al*. Thermal shock resistance of YSZ, YSZ-Al_2O_3 and YSZ-Al_2O_3/YSZ coatings. *Vacuum* 2019, **162**: 150-155.

[14] Levit M, Grimberg I, Weiss BZ. Residual stresses in ceramic plasma-sprayed thermal barrier coatings: Measurement and calculation. *Mater Sci Eng A* 1996, **206**: 30-38.

[15] Zhang XC, Watanabe M, Kuroda S. Effects of residual stress on the mechanical properties of plasma-sprayed thermal barrier coatings. *Eng Fract Mech* 2013, **110**: 314-27.

[16] Song XM, Zhang JM, Lin CC, *et al*. Microstructures and residual strain/stresses of YSZ coatings prepared by plasma spraying. *Mater Lett* 2019, **240**: 217-220.

[17] Xu YJ, Guo XJ, Lin CC, *et al*. Thermal Properties and Microstructures Analysis of YSZ and YSZ-Al_2O_3 Thermal Barrier Coatings. *J Therm Spray Technol* 2020, **29**: 574-581.

[18] Song XM, Xu YJ, Ding Y, *et al.* Study of microstructure, electronic structure and thermal properties of Al_2O_3-doped tetragonal YSZ coatings. *Appl Surf Sci* 2021, **542**: 148553.

[19] Wang Y, Bai Y, Yuan T, *et al*. Failure analysis of fine-lamellar structured YSZ based thermal barrier coatings with submicro/nano-grains. *Surf Coatings Technol* 2017, **319**: 95-103.

[20] Salvati E, Korsunsky AM. An analysis of macro- and micro-scale residual stresses of Type I, II and III using FIB-DIC micro-ring-core milling and crystal plasticity FE modelling. *Int J Plast* 2017, **98**: 123-138.

[21] Lee EJ, Chen Z, Noh HJ, *et al*. Development of microstrain in aged lithium transition metal oxides. *Nano Lett* 2014, **14**: 4873–4880.

[22] Wan VVC, Cuddihy MA, Jiang J, *et al.* An HR-EBSD and computational crystal plasticity investigation of microstructural stress distributions and fatigue hotspots in polycrystalline copper. *Acta Mater* 2016, **115**: 45-57.

[23] Jin L, Ni L, Yu Q, *et al.* Thermal cyclic life and failure mechanism of nanostructured 13 wt%Al_2O_3 doped YSZ coating prepared by atmospheric plasma spraying. *Ceram Int* 2012, **38**: 2983-2989.

[24] Yang J, Jiang W. Influence of welding residual stress on stress intensity factor of two-dimensional cracks. *Adv Mater Res* 2011, **299-300**: 966-969.

[25] Zhu X, Huang YL, Zheng W, et al. Crystallinity, Stresses, and Cracks of YSZ Coatings Characterized by SEM-EBSD-Raman Spectroscopy. *J Therm Spray Technol* 2020, **29**: 995-1001.

[26] Mao W, Yu Y. Effect of elastic reaction stress on plastic behaviors of grains in polycrystalline aggregate during tensile deformation. *Mater Sci Eng A* 2004, **367**: 277–281.

[27] Lu M, Wang F, Zeng XG, *et al*. Cohesive zone modeling for crack propagation in polycrystalline NiTi alloys using molecular dynamics. *Theor Appl Fract Mech* 2020, **105**: 102402.

[28] Schelling PK, Phillpot SR, Wolf D, *et al.* Mechanism of the Cubic-to-Tetragonal Phase Transition in Zirconia and Yttria-Stabilized Zirconia by Molecular-Dynamics Simulation. *J Am Ceram Soc* 2001, **84**: 1609-1619

[29] Messerschmidt U, Baither D, Baufeld B, *et al*. Plastic deformation of zirconia single crystals: A review. *Mater Sci Eng A* 1997, **233**: 61-74..

Figures

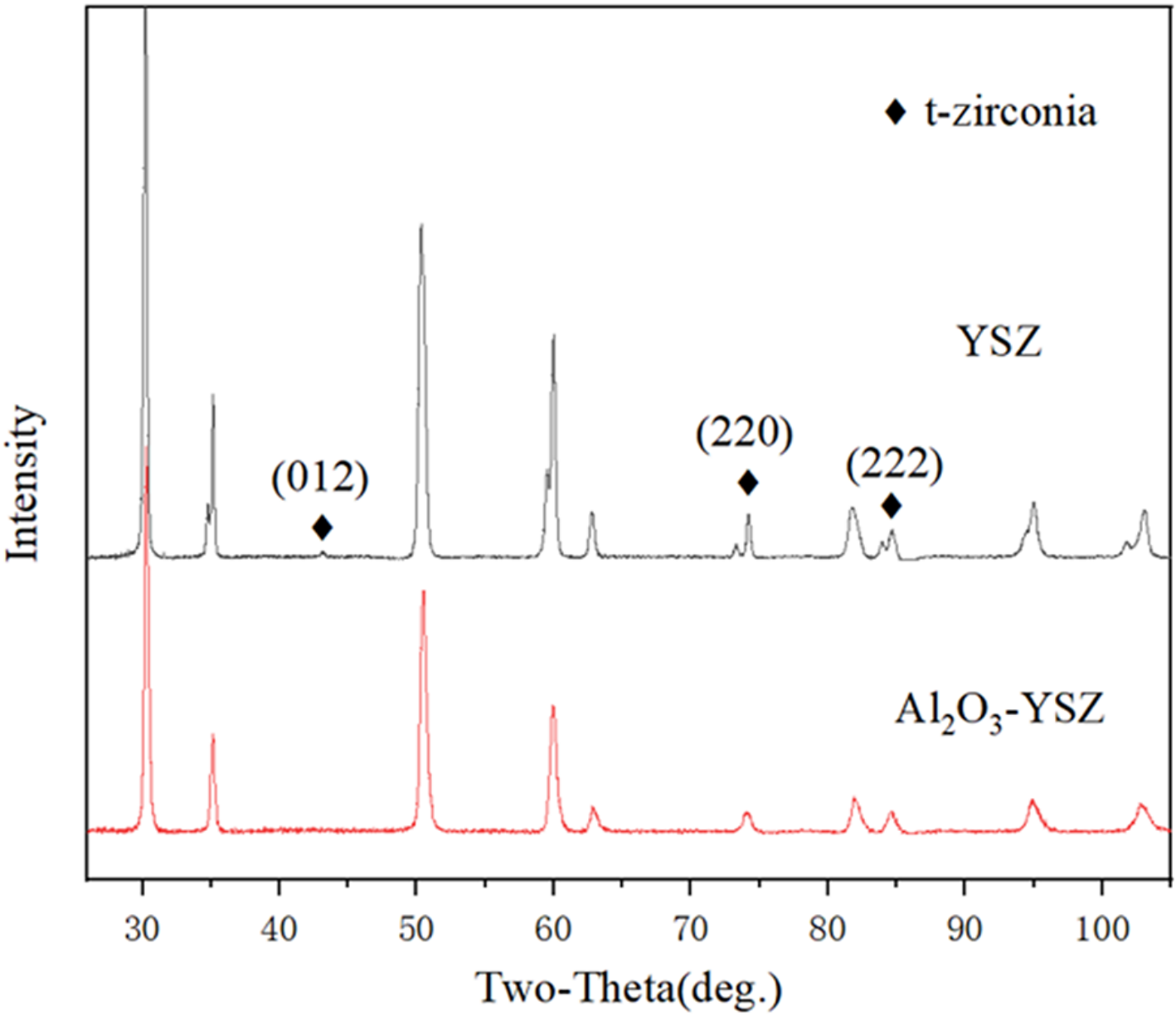

Figure 1

XRD patterns of the as-sprayed YSZ and Al2O3-YSZ coatings.

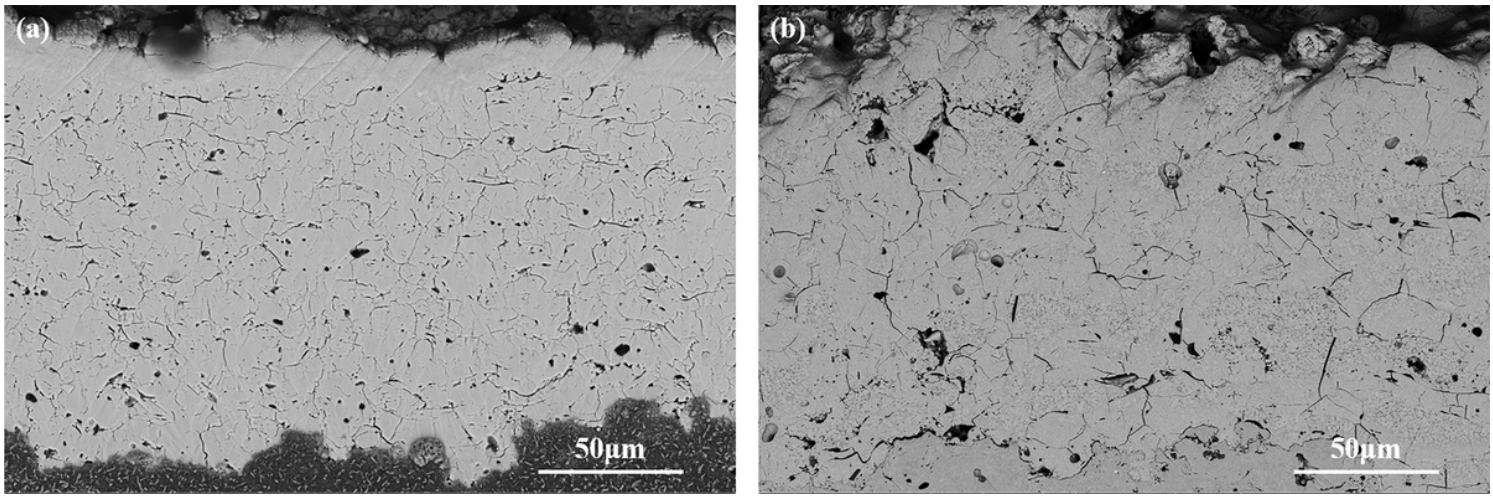

Figure 2

SEM images from cross-sections of (a) YSZ coatings and (b) Al2O3-YSZ coatings.

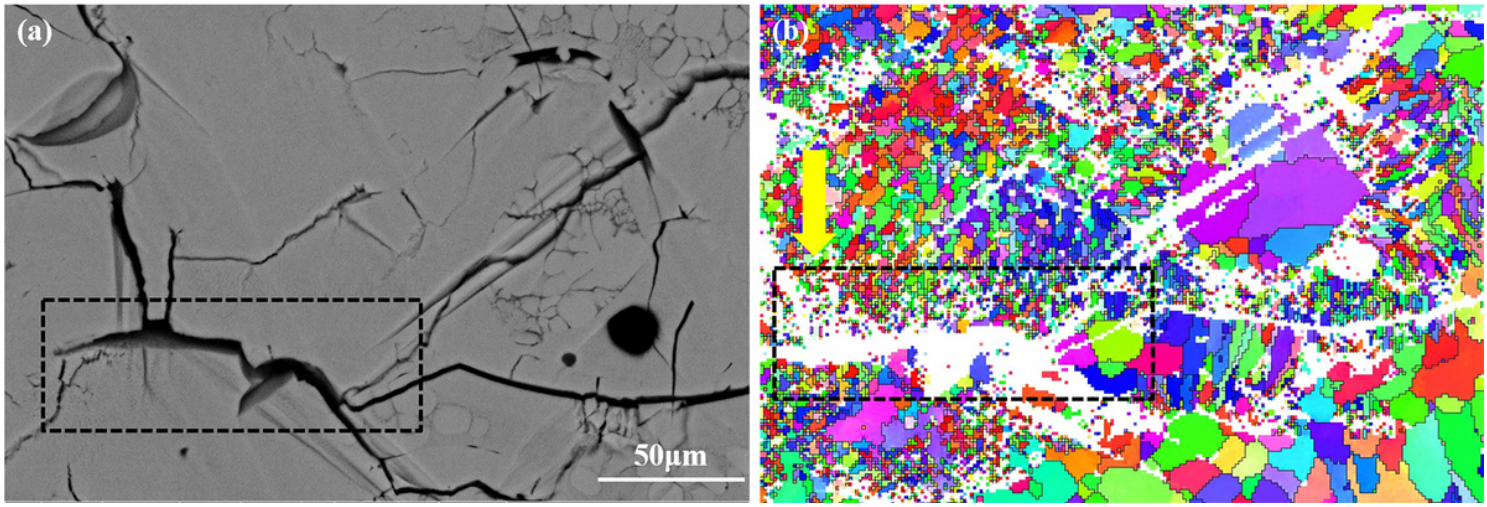

Figure 3

(a) SEM image and (b) EBSD image of Al2O3-YSZ coatings.

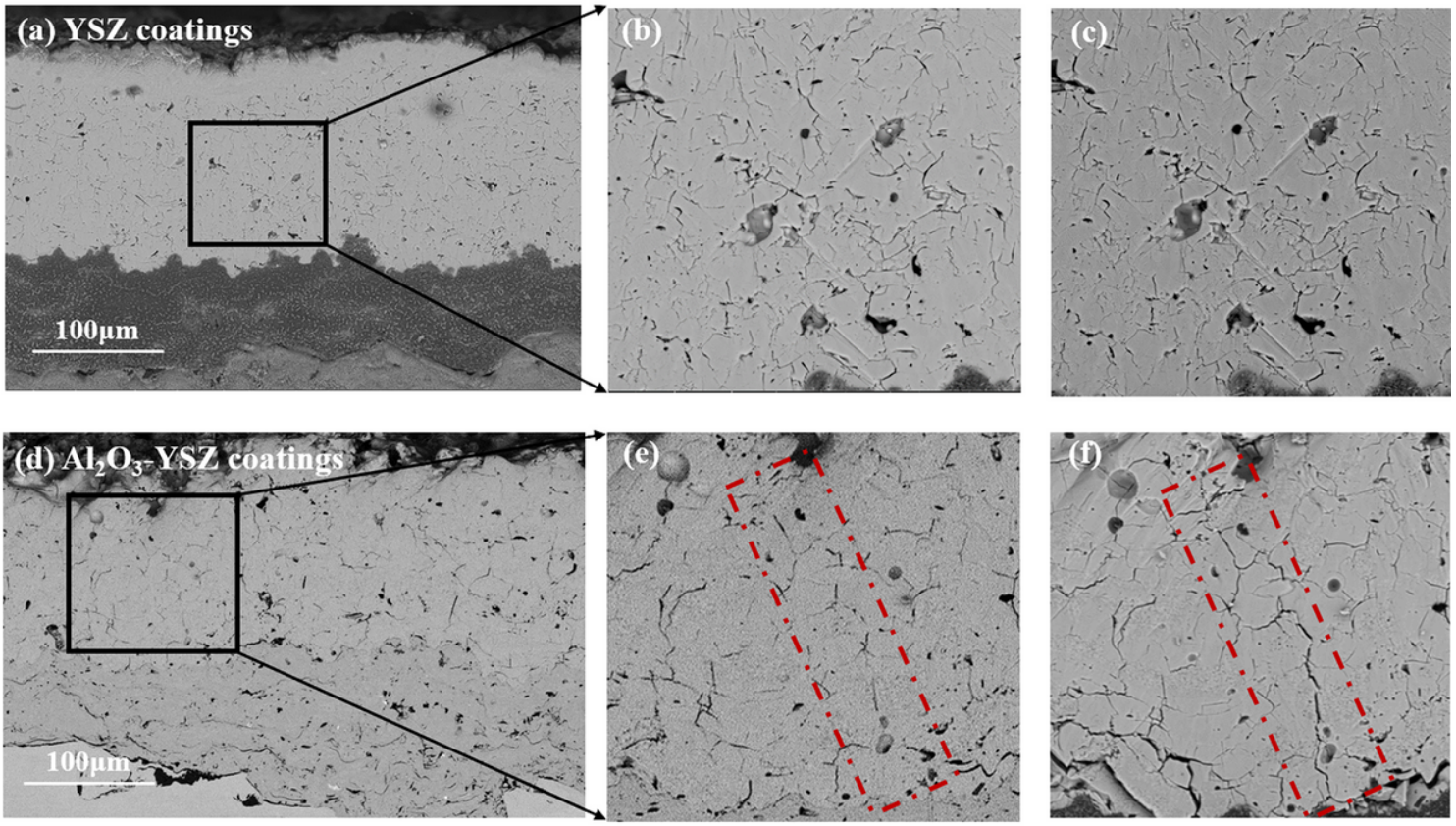

Figure 4

SEM images of polished cross-sections of different coatings before and after thermal cycles: (a)(b)(d)(e) before thermal cycles; (c)(f) after five thermal cycles.

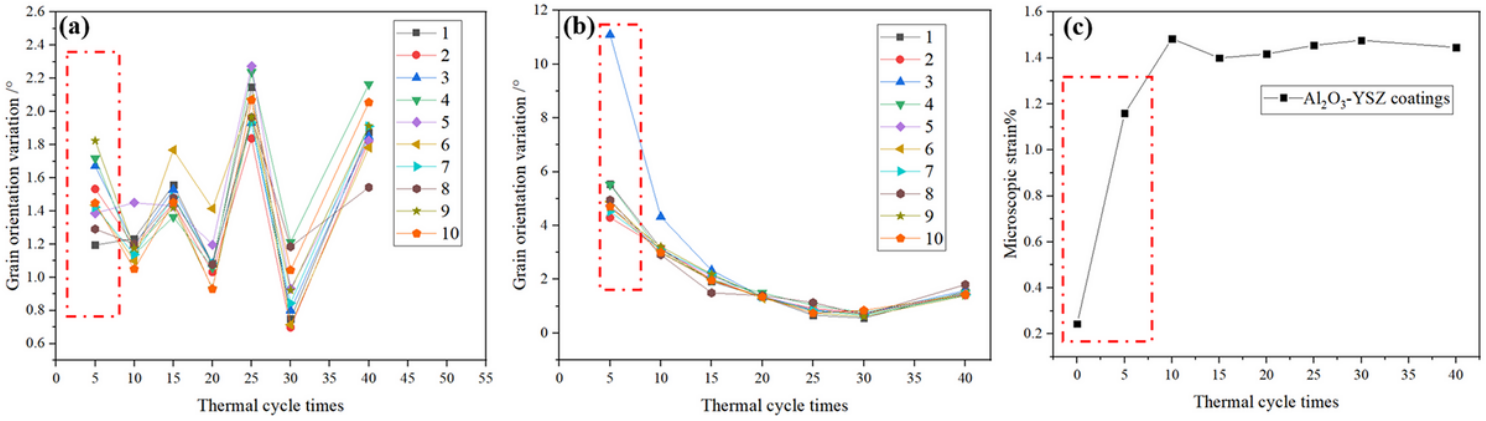

Figure 5

Grain orientation variation trend of (a) YSZ coating and (b) Al2O3-YSZ coating during thermal cycles; (c) Microscopic strain of Al2O3-YSZ coating during thermal cycles.

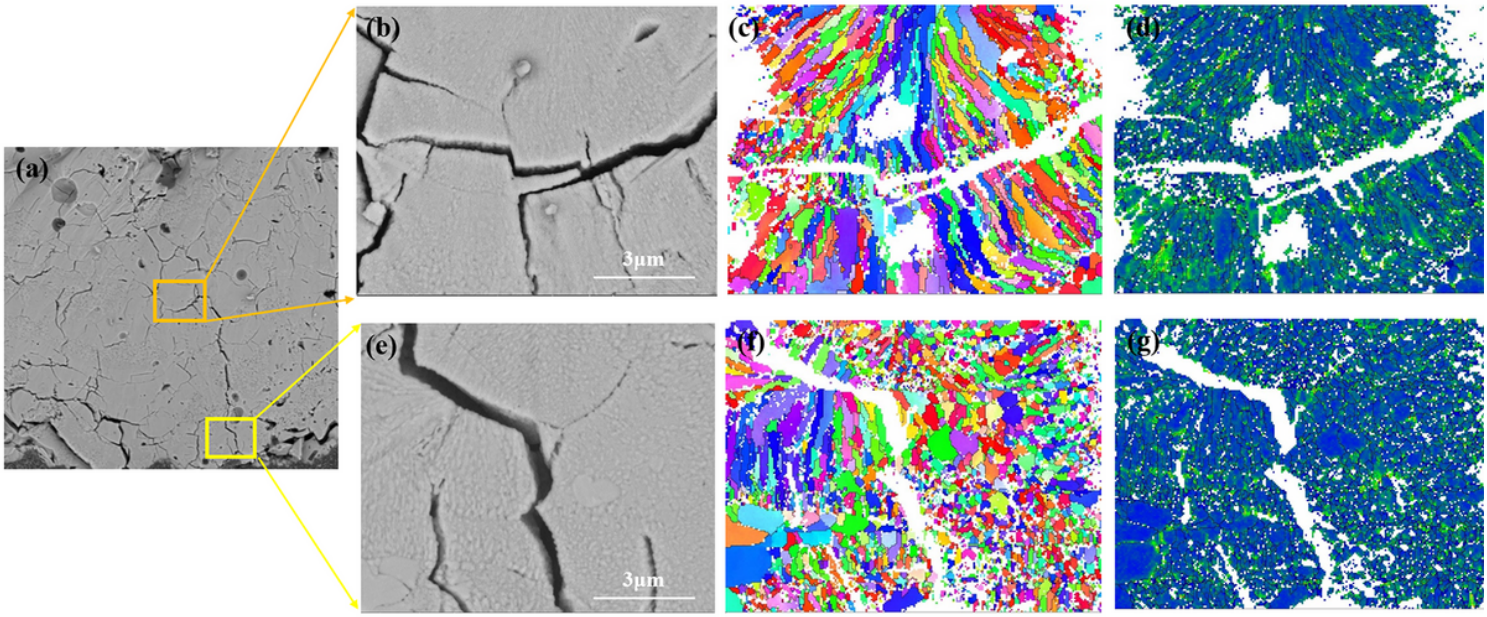

Figure 6

(a) SEM image of Al2O3-YSZ coating; (b)(e) Two areas selected near the crack: site 1 and site 2; (c)(f) EBSD image and (d)(g) Local misorientation distribution images of site 1 and site 2.

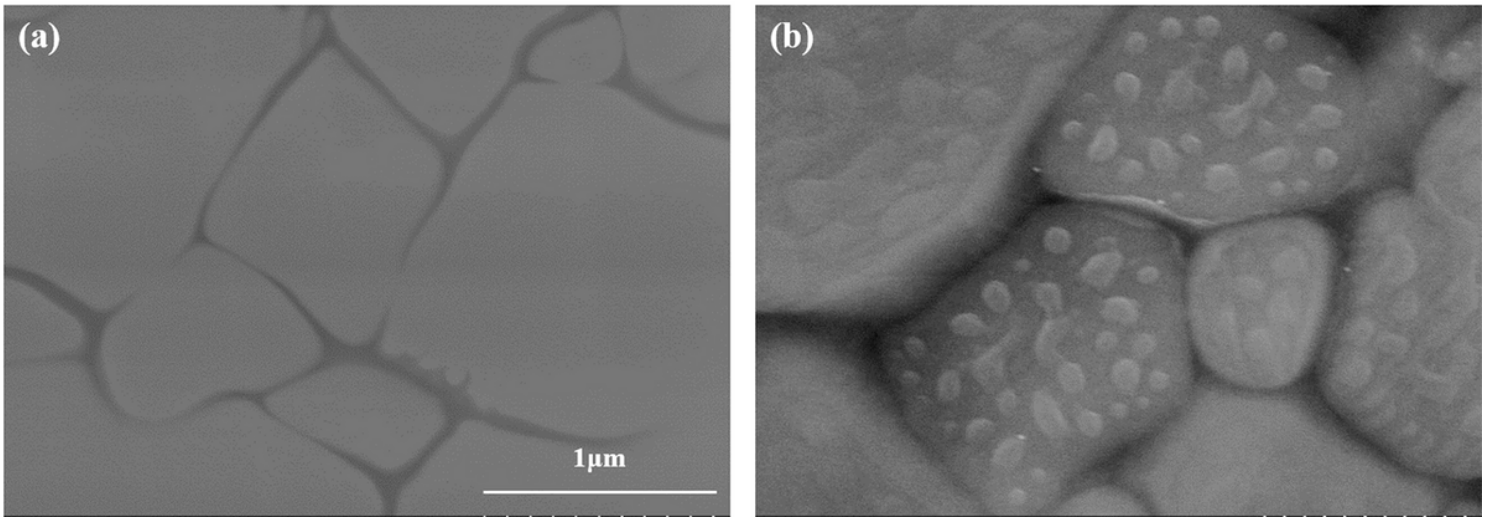

Figure 7

SEM images of equiaxed grains in Al2O3-YSZ coatings (a) before thermal cycles; (b) after thermal cycles.

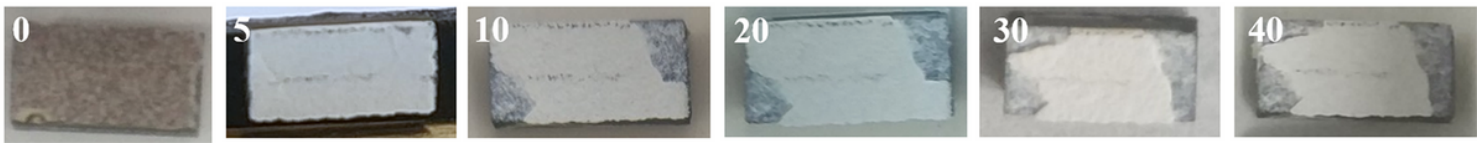

Figure 8

Image of Al2O3-YSZ coatings during thermal cycling.

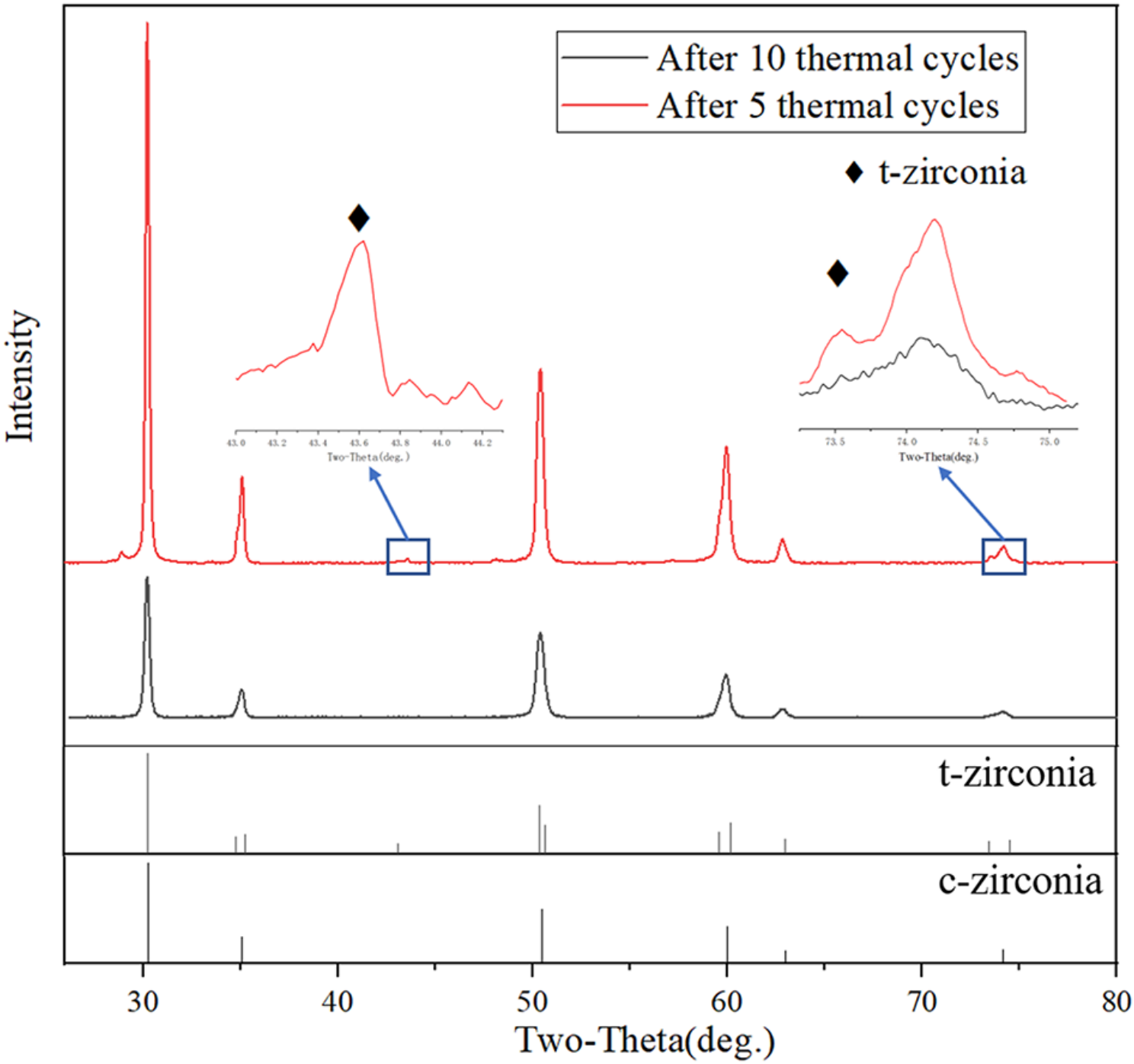

Figure 9

XRD patterns of Al2O3-YSZ coatings after 5 and 10 thermal cycles.